2014 International Joint Conference on Neural Networks (IJCNN)
July 6-11, 2014, Beijing, China

Dynamic Modeling of an Ostraciiform Robotic Fish Based on Angle of Attack Theory

Wei Wang, Guangming Xie and Hong Shi

Abstract— **This paper focuses on the dynamic modeling of a self-propelled, multimodal ostraciiform robotic fish, whose three active joints (two pectoral fins and one caudal fin) are actuated by a Central Pattern Generator (CPG) controller. Compared with other dynamic modes for robotic fish, we introduce angle of attack (AoA) theory on the fish modeling, which can be used to further explore the relationship between swimming efficiency and AoA of robotic fish. First, by using the quasi-steady wing theory, AoA of the oscillatory fins are explicitly derived. Then, with the simplification of the robot as a multi-rigid-body mechanism, AoA-based fluid forces acting on the oscillatory fins of the robot are further approximately calculated in a three-dimensional context. Next, by importing the driving signals (generated by CPG control law) into a Lagrangian function, the differential-algebraic equations are employed to establish a hydrodynamic model for steady swimming of the ostraciiform robotic fish for the first time. Finally, comparative results between simulations and experiments for forward and turning gaits of the robot are systematically conducted to show the effectiveness of the built AoA-based dynamic model.**

I. Introduction

With the increasing demand of ocean explorations, biomimietic swimming robots have been an active area for both roboticists and biologists over the last several decades [1]. Compared to traditional screw-propeller based underwater vehicle, the bio-inspired aquatic robots would be more maneuverable and silent when they are operating. This enables a good integration with the underwater habitats and impacts the surroundings at a minimum degree. Moreover, biomimetic robotic fish would be easily recognized by and interacted with aquatic animals, which could contribute to the migration, hedging and foraging of fish school [2].

As one of the most fundamental issues of biomimietic underwater robots, hydrodynamic modeling for fish and their robotic counterpart has been extensively investigated in the literature. At early years, Lighthill's elongated body theory [3] and his large-amplitude elongated-body theory [4] were successively built and widely used in force analysis of fish swimming. In 1990's, Triantafyllou's group [5] studied the wake theories of oscillating foil propulsion to reveal the underlying vorticity control mechanisms in fish swimming. Recently, more and more dynamic models for the free swimming robotic fish have been proposed and contrasted with the conducted experiments. For instance, McIsaac and Ostrowski [6] proposed a Lagrangian-based dynamic model for the eel-like swimming robot. Using the geometric methods, Morgansen et al. [7] developed a 3D equations of motion for the robotic fish with independently actuated rigid pectoral fins and a tail. Yu et al. [8] established a dynamic system for a carangiform multi-joint robotic fish, which was used to seek backward swimming patterns of the robot. By integrating classical Euler-Bernoulli beam theory and Morisons formula, Porfiri'group have developed an integrated modeling framework for predicting the robot's static thrust production [9]. However, most of the proposed dynamic models were developed for anguilliform and carangifom robotic fish. An example can be found in Deng's group [10], where a Newton-Euler based dynamic model was built for a ostraciiform boxfish-like robot with a pair of pectoral fins. In addition, although the AoA is a widely recognized factor that counts a great deal in thrust formulation of fish swimming [11], [12], rarely dynamic models have explicitly derived the expression of AoA and utilized it in the dynamic modeling of robotic fish in the literature.

Based on our previous projects on the use of CPGs for controlling the robotic fish in kinematics [13], this paper aims at establishing a AoA-based dynamic model for a CPG-controlled ostraciiform robotic fish, which, in conjunction with the CPG controller, is able to predict mechanical behaviors of the robot and guide the search for CPG parameters and gaits optimization of the robot. Specifically, we derive a explicit expression of AoA for the oscillatory fins of robotic fish. Using the Lagrangian equations, we then develop an AoA-based differential-algebraic dynamic model for an ostraciiform robotic fish in a three-dimensional context for the first time. Compared with other dynamic models for robotic fish, the AoA-based model can be used to further explore the relationship between the hydrodynamic forces and the angle of attack of fins. Finally, comparative results between simulations and experiments are systematically conducted to demonstrate the effectiveness of the AoA-based dynamic model.

The reminder of this paper is organized as follows. Section II gives an overview of the ostraciiform robotic fish and its CPG controller. The AoA-based fluid forces and dynamic model are exhaustively derived in a three-dimensional context in Section III. Simulations and experiments are provided in Section IV. Conclusion and future work are given at the end of this paper.

This work was supported by Beijing Municipal Commission of Education Science and Technology Program (KM201310017006).

W. Wang and Guangming Xie are with the Intelligent Control Laboratory, College of Engineering, Peking University, Beijing 100871, China wangweiw4y4@pku.edu.cn;xiegming@pku.edu.cn

Hong Shi is with the Department of Mathematics and Physics, Beijing Institute of Petrochemical Technology, Beijing 102617, China shihong@bipt.edu.cn

978-1-4799-1484-5/14/$31.00 ©2014 IEEE

II. The Boxfish-like Robot and its CPG Controller

A. Overview of the Ostraciiform Robot

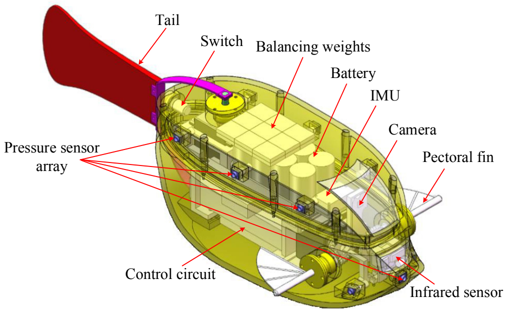

Fig. 1. Configurations of the boxfish-like robot.

Fig. 1 illustrates a newly developed autonomous/wireless-controlled ostraciiform robotic fish prototype, which, as a upgrade version of the robot in [13], consists of a well-streamlined main body, two degree-of-freedom paired pectoral fins and one degree-of-freedom caudal fin. Mass distribution of the robot is attentively considered in mechanical design, which makes the robot be able to expediently perform multimodal swimming gaits involving forward and backward swimming, turning, pitching and rolling. Moreover, diversified sensors are equipped on the robot, including camera, IMU, pressure sensor array and infrared sensor, to make it possible to realize fully autonomous swimming in a wild environment.

B. The CPG Controller

The CPG controller has the ability to deal with redundancies and perform smooth transitions while only receiving simple control signals. Therefore, it is suitable for locomotion control of robotic fish which performs rhythmic oscillations. The CPG controller adopted here takes the form [13], [14]

$$\ddot{k}_i = \gamma\left(\gamma(K_i - k_i) - 2\dot{K}_i\right) \tag{1a}$$

$$\ddot{x}_i = \eta\left(\eta(X_i - x_i) - 2\dot{x}_i\right) \tag{1b}$$

$$\dot{\zeta}_i = 2\pi f_i + \sum_j \mu_{ij} k_j sin(\zeta_j - \zeta_i - \varphi_{ij}) \tag{1c}$$

$$\theta_i = x_i + k_i \sin(\zeta_i) \tag{1d}$$

where variable θ_i is the output signal of the i^{th} oscillator. It is used to drive the corresponding fin joint of robotic fish. Note that θ_i is as well as the imported signal for the following AoA-based dynamic model and $i = 1, 2, 3$ respectively represent left pectoral fin, right pectoral fin and caudal fin of the robot. k_i, x_i, and ζ_i are state variables that represent amplitude, offset, and phase of the i^{th} oscillator, respectively. f, K_i, X_i and φ_{ij} are control parameters for the desired frequency, amplitude and offset of the oscillations and $\varphi_{ij} = 0$ in this paper. The coupling effects among oscillators are determined by the constant positive gains, μ_{ij}, γ and η. More details of the CPG controller for robotic fish can be found in [13].

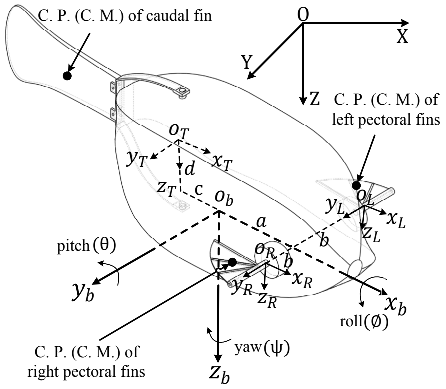

Fig. 2. The earth-fixed inertial frame, body-fixed frame and three fin-fixed frames used in this paper.

III. Three-dimensional Hydrodynamic Modeling

A. Kinematic Analysis

The robotic fish is regarded as a multi-rigid-body system with four components: one main body and three rotatable flippers. Thus, to clearly describe kinematics of the system, five rectangular coordinate systems are established, as exhibited in Fig. 2. Specifically, the earth-fixed initial frame $\{X,Y,Z\}$ and body-fixed frame $\{x_b, y_b, z_b\}$ are used to express interactions between the robotic fish and its surrounding fluids. Origin of the frame $\{x_b, y_b, z_b\}$ is placed at center of mass (C. M.) of the robot, which is assumed to coincide with its center of buoyancy (C. B.). The frames $\{x_i, y_i, z_i\}$ ($i =$ 1, 2, 3) are used to describe motions of the left pectoral fin, right pectoral fin and tail fin, respectively. Unless otherwise stated, $i =$ 1, 2, 3 stand for abbreviations L, R and T, which respectively represent left pectoral fin, right pectoral fin and the tail of the robotic fish. The origins O_i are expressed in the body-fixed frame as $\mathbf{b}_{1b} = [a\ -b\ 0]^T$, $\mathbf{b}_{2b} = [a\ b\ 0]^T$ and $\mathbf{b}_{3b} = [c\ -d\ 0]^T$. The yaw angle ψ, pitch angle θ and roll angle ϕ describe rotations about frame $\{x_b, y_b, z_b\}$ at a sequence of $z_b - y_b - x_b$. Note that all the angles defined in this paper abide right hand rule. That is, the angle will take positive value if it represents a counter-clockwise rotation from the formulary initial status when observed from one point laying on positive part of the stationary axis.

Traditionally, the total forces acting on each fin are supposed to act at center of pressure (C. P.) of the fin. For the convenience of dynamic analysis, C. P. of the fins are assumed to be coincident with their corresponding C. M.. At a result, position of the robot takes the form $\mathbf{r}_b = [x_b\ y_b\ z_b]^T$ and C. P. of each fin is defined as $\mathbf{r}_i^i = [x_i^i\ y_i^i\ z_i^i]^T$, where subscript $i =$ 1, 2, 3 represent L, R and T and superscript i stand for the position expresses in the related frame $\{x_i, y_i, z_i\}$.

From Fig. 2, the position of each fin in frame $\{X,Y,Z\}$ can be expressed as:

$$\mathbf{r}_i = \mathbf{R}\mathbf{r}_i^b + \mathbf{r}_b \tag{2}$$

where $\mathbf{R}$ is the transform matrix from body-fixed frame to earth-fixed frame; $\mathbf{r}_i^b$ is the position of each fin expressed in the body-fixed frame and takes the form $\mathbf{r}_i^b = \mathbf{H}_{ib}\mathbf{r}_i^i + \mathbf{b}_{ib}$

where $\mathbf{H}_{ib}$ represents the transfrom matrix from the i^{th} fin-fixed frame to body-fixed frame. Then, we can derive the velocities of three fins relative to water in the earth-fixed frame, i. e., $\mathbf{v}_i = \dot{\mathbf{r}}_i$.

Similarly, the angular velocity of the robot and the robot's three fins are calculated. Based on the relationship $\dot{\mathbf{R}} = \mathbf{R}\hat{\boldsymbol{\omega}}_b$ where $\hat{\boldsymbol{\omega}}_b$ is the hat operator of $\boldsymbol{\omega}_b$, the angular velocity of the robot is easily derived and takes the form

$$\boldsymbol{\omega}_b = \begin{bmatrix} 1 & 0 & -\sin\theta \\ 0 & \cos\phi & \sin\phi\cos\theta \\ 0 & -\sin\phi & \cos\phi\cos\theta \end{bmatrix} \begin{bmatrix} \dot{\phi} \\ \dot{\theta} \\ \dot{\psi} \end{bmatrix} \tag{3}$$

Next, the angular velocity of each fin relative to the earth-fixed frame contains two parts: one is produced by rotation of the moving fin, the other is derived by rotation of the main body, namely:

$$\boldsymbol{\omega}_i = \boldsymbol{\omega}_b + \boldsymbol{\omega}_{i,bs} \tag{4}$$

where $\boldsymbol{\omega}_{i,bs}$ is the angular velocity caused by rotation of the moving fin. It takes the form $\boldsymbol{\omega}_{i,bs} = \mathbf{R}\boldsymbol{\omega}^i_{i,bs}$ where $\boldsymbol{\omega}^i_{i,bs}$ equals to $[0\ \dot{\theta}_L\ 0]$, $[0\ \dot{\theta}_R\ 0]$ and $[0\ 0\ \dot{\theta}_T]$ for $i = 1, 2, 3$. Finally, the angular velocity of each fin relative to their corresponding moving frame $\{x_i, y_i, z_i\}$ is expressed as follows:

$$\boldsymbol{\omega}^i_i = \mathbf{H}^T_{ib}\mathbf{R}^T\boldsymbol{\omega}_i \tag{5}$$

B. Hydrodynamic Force Approximation

As ostraciiform fish advances just by oscillating combinations of its flexible fins, most of the thrust will be generated by its oscillatory fins. Similar to natural boxfish, thrust of the boxfish-like robot is assumed to be generated mainly by its three fins. We also assume that the flow around the fish is incompressible, inviscid and irrotational. Moreover, pectoral fins are modeled as rectangle while the tail fin is regarded as ladder-shaped. The span and chord length of each fin will be provided in Table II (in the later section). Thus, we use the quasi-steady wing theory to approximately calculate fluid forces (lift and drag) acting on the moving hydrofins. Moreover, when the robot is operating, it suffers a sustained drag on the whole body, which is assumed to act on C. M. of main body.

1) Lift and drag acting on the moving fins: Each fin of the robot is regarded as a very thin plate and then, the lift and drag acting on the moving fins are illustrated in Fig. 3, where v_{bf} is the relative speed between the robot and fluid, i. e., the magnitude of the robot's velocity $\mathbf{v}_b$, v_{if} is the fin speed relative to the fluid taking the form $v_{if} = v_{fi} = |\mathbf{v}_i|$, l_i is the distance from C. P. of the i^{th} fin to the rotational axis, $F_{L,i}$ and $F_{D,i}$ are the lift and drag acting on the i^{th} fin, respectively.

For both fish and robotic fish, AoA plays a vital role when they are swimming. Generally, AoA is the angle between the reference line (the fin of the robot here) and the oncoming flow, as presented in Fig. 3. Actually, different parts of the fin along chordwise take varied values for the reason that the linear speed caused by rotation of the fin is not the same in different parts. Nevertheless, for the purpose of primarily

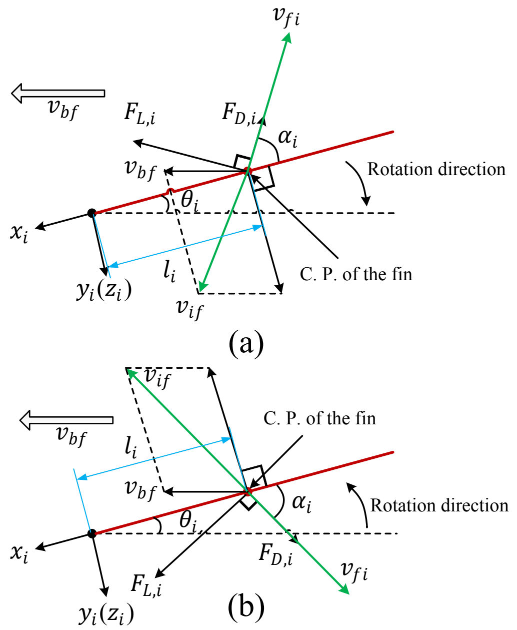

Fig. 3. The definition of AoA of the fins, the lift and drag acting on the oscillatory fins. Red lines stand for the corresponding moving fins. For i =1, 2, the figure is observed from side view while for $i = 3$, the figure is observed from top view. (a) The fin oscillates in one direction of one beating period; (b)The fin oscillates in the opposite direction of a beating period.

verifying effectiveness of the explicitly AoA-based force analysis and the dynamic model, only AoA of C. P. of the fin is concerned and calculated in this paper. Without loss of generality, the sign of AoA also defines to obey right-handed rule. Note that AoA is an acute angle and it is derived from Fig. 3 and takes the form

$$\alpha_i = \arctan\frac{\beta_i l_i \dot{\theta}_i \cos\theta_i}{v_{bf} + \beta_i l_i \dot{\theta}_i \sin\theta_i} + \theta_i \tag{6}$$

where α_i is the AoA of C. P. of the i^{th} fin and β_i is regulator to reflect the fact that the beating speed of flexible fin would decrease compared to the rigid one. In the paper, $\beta_i = 0.6$ is adopted as the relative flexibility of the used fins. Note that although derivation of the AoA is in the context of forward swimming, it is effective to a great extent for other swimming gaits. Moreover, the AoA for serially connected multi-joint robotic fish is more complicated and is worthy of further investigation.

Then, by using the quasi-steady wing theory, we can derive the AoA-based lifts and drags acting on the three fins [15], namely

$$F_{L,i} = 0.5\rho C_{Lmax} S_i v^2_{if} sin(2|\alpha_i|) \tag{7}$$

$$F_{D,i} = 0.5\rho C_{Dmax} S_i v^2_{if}(1 - cos(2|\alpha_i|)) \tag{8}$$

where ρ is the density of the fluid, S_i is the fin area, C_{Lmax} and C_{Dmax} are respectively the maximum lift and drag coefficients, where $C_{Lmax} = 2.2$ and $C_{Dmax} = 0.6$ in this paper [15].

These fluid forces are divided into thrust components in the three directions of body-fixed frame. From Eqs. 7 and 8,

$\mathbf{F}_i^b$ are written as,

$$\mathbf{F}_L^b = \begin{bmatrix} \cos\theta_L & 0 & \sin\theta_L \\ 0 & 1 & 0 \\ -\sin\theta_L & 0 & \cos\theta_L \end{bmatrix} \begin{bmatrix} -\cos\alpha_L & 0 & sgn(\dot{\theta}_L)\sin\alpha_L \\ 0 & 1 & 0 \\ -\sin\alpha_L & 0 & -sgn(\dot{\theta}_L)\cos\alpha_L \end{bmatrix} \begin{bmatrix} F_{D,L} \\ 0 \\ F_{L,L} \end{bmatrix} \quad (9a)$$

$$\mathbf{F}_R^b = \begin{bmatrix} \cos\theta_R & 0 & \sin\theta_R \\ 0 & 1 & 0 \\ -\sin\theta_R & 0 & \cos\theta_R \end{bmatrix} \begin{bmatrix} -\cos\alpha_R & 0 & sgn(\dot{\theta}_R)\sin\alpha_R \\ 0 & 1 & 0 \\ -\sin\alpha_R & 0 & -sgn(\dot{\theta}_R)\cos\alpha_R \end{bmatrix} \begin{bmatrix} F_{D,R} \\ 0 \\ F_{L,R} \end{bmatrix} \quad (9b)$$

$$\mathbf{F}_T^b = \begin{bmatrix} \cos\theta_T & -\sin\theta_T & 0 \\ \sin\theta_T & \cos\theta_T & 0 \\ 0 & 0 & 1 \end{bmatrix} \begin{bmatrix} -\cos\alpha_T & sgn(\dot{\theta}_T)\sin\alpha_T & 0 \\ \sin\alpha_T & sgn(\dot{\theta}_T)\cos\alpha_T & 0 \\ 0 & 0 & 1 \end{bmatrix} \begin{bmatrix} F_{D,T} \\ F_{L,T} \\ 0 \end{bmatrix} \quad (9c)$$

where $\mathrm{sgn}(\cdot)$ is a signum function and takes the form

$$\mathrm{sgn}(t) = \begin{cases} -1, & \text{if} \quad t < 0; \\ 0, & \text{if} \quad t = 0; \\ 1, & \text{otherwise.} \end{cases} \quad (10)$$

Thus, the AoA-based forces acting on the three fins are expressed in the earth-fixed frame $\mathbf{F}_i = \mathbf{R}\mathbf{F}_i^b$.

2) Force on the rigid body: As C. M of the robot is coincident with C. B of the robot and density of the robot is identical to water, the moments result from gravity and buoyancy are zero all the time. Therefore, the main body only suffers a effective drag. Specifically, the drags in the $x_b - y_b$ plane and $x_b - y_b$ are calculated and the drag in the $y_b - z_b$ plane is neglected for the reason that the robot can not perform lateral movement with its structural configurations. As a result, the drag $\mathbf{F}_D^b = [F_{D,xy}^b \ F_{D,xz}^b \ 0]^T$ can be expressed as follows:

$$F_{D,xy}^b = 0.5\rho C_{D,xy} S_{xy} ({v_x^b}^2 + {v_y^b}^2) \quad (11)$$

$$F_{D,xz}^b = 0.5\rho C_{D,xz} S_{xz} ({v_x^b}^2 + {v_z^b}^2) \quad (12)$$

$$F_{D,yz}^b = 0 \quad (13)$$

where ρ is the density of fluid, S_{xy} and S_{xz} are the cross-section areas of the body in the $y_b - z_b$ and $x_b - y_b$ planes, respectively. Similarly, $C_{D,xy}$ and $C_{D,xz}$ are the drag coefficients of the fish body in the corresponding planes where $C_{D,xy} = 0.255$ and $C_{D,xz} = 0.57$. The speed v_x^b, v_y^b and v_z^b are magnitudes of fish speed divided into the x_b, y_b and z_b axes, respectively. Similarly, the drag can be expressed in the earth-fixed frame $\mathbf{F}_D = \mathbf{R}\mathbf{F}_D^b$.

C. Lagrangian Dynamic Modeling

As the gravity of the robot is equal to its buoyancy, the potential energy (E) is constant. The kinetic energy comprises translational kinetic energy and rotational kinetic energy for the multi-rigid-body system with respect to the inertial coordinate system. Therefore, Lagrangian function for the robotic system expresses as follows:

$$\begin{aligned} L_f &= \frac{1}{2} m_b {\mathbf{v}_b}^T \mathbf{v}_b + \frac{1}{2} \boldsymbol{\omega}_b^T I_b \boldsymbol{\omega}_b \\ &+ \sum_{i=1}^{3} \frac{1}{2} m_i {\mathbf{v}_i}^T \mathbf{v}_i + \sum_{i=1}^{3} \frac{1}{2} {\boldsymbol{\omega}_i^i}^T I_i \boldsymbol{\omega}_i^i - E \end{aligned} \quad (14)$$

where m_b and m_i are mass of the main body and the i^{th} fin of robotic fish; $\mathbf{v}_b$, $\mathbf{v}_i$, $\boldsymbol{\omega}_b$ and $\boldsymbol{\omega}_i^i$ are velocities and angular velocities of the multi-rigid-body system which have been defined and derived at the fore of this paper. I_b is inertia tensor of the robot respect to its three principal axes. Similarly, I_i is inertia tensor of the i^{th} fin respect to its three moving axes. Note that only diagonal elements of I_b and I_i takes non-zero values. In order to compute L_f, x_b, y_b, z_b, ϕ, θ, ψ, θ_L, θ_R and θ_T are chosen as the generalized coordinates. Because $\theta_L = x_L + k_L \sin(\zeta_L)$, $\theta_R = x_R + k_R \sin(\zeta_R)$, $\theta_T = x_T + k_T \sin(\zeta_T)$ are the system input of the dynamic model, let $X = x_b$, $Y = y_b$, $Z = z_b$, $\Phi = \phi$, $\Theta = \theta$ and $\Psi = \psi$, and the Lagrange equations can be given by:

$$\begin{cases} Q_X &= \dfrac{d}{dt}\dfrac{\partial L_f}{\partial \dot{X}} - \dfrac{\partial L_f}{\partial X} \\ Q_Y &= \dfrac{d}{dt}\dfrac{\partial L_f}{\partial \dot{Y}} - \dfrac{\partial L_f}{\partial Y} \\ Q_Z &= \dfrac{d}{dt}\dfrac{\partial L_f}{\partial \dot{Z}} - \dfrac{\partial L_f}{\partial Z} \\ Q_\Phi &= \dfrac{d}{dt}\dfrac{\partial L_f}{\partial \dot{\Phi}} - \dfrac{\partial L_f}{\partial \Phi} \\ Q_\Theta &= \dfrac{d}{dt}\dfrac{\partial L_f}{\partial \dot{\Theta}} - \dfrac{\partial L_f}{\partial \Theta} \\ Q_\Psi &= \dfrac{d}{dt}\dfrac{\partial L_f}{\partial \dot{\Psi}} - \dfrac{\partial L_f}{\partial \Psi} \end{cases} \quad (15)$$

where Q_i is the generalized force and takes the expression

$$Q_i = \sum_{j=1}^{4} \mathbf{F}_j \cdot \frac{\partial \mathbf{r}_j}{\partial q_i} \quad (16)$$

where F_j is the hydrodynamic force on the j^{th} rigid body of the robotic fish where $j = 1, 2, 3, 4$ represent the left pectoral fin, right pectoral fin, caudal fin and the main body of the robot. $\mathbf{r}_j$ is the position of the j^{th} rigid body and q_i is the i^{th} generalized coordinate. θ_L, θ_R and θ_T are the joint angles served by CPG controller in Eqn. 1. The parameters measured and estimated from the physical robot are listed in Table II. It is apparent that the Lagrange equations here are differential algebraic equations (DAEs) and simulations are performed in the Mathematica environment.

TABLE I
PARAMETERS OF THE ROBOT FOR THE DYNAMIC SIMULATION

Items	e_i (mm)	h_i (mm)	m_i (kg)	S_i (mm^2)	$I_i(I_{xx}, I_{yy}, I_{zz})$ (10^{-4}kg$\cdot$ mm^2)
Left (i=1)	100	60	0.025	5600	0.300, 8.33, 1.13
Right (i=2)	100	60	0.025	5600	0.300, 8.33, 1.13
Tail (i=3)	140	100	0.040	8750	0.333, 8.01, 7.68
Body (i=4)	×	×	3.093	11200(S_{xy}) 30500(S_{xz})	1045, 1049, 321

IV. SIMULATIONS AND EXPERIMENTS

In order to evaluate the suitability of the model developed in Section III, forward and turning gaits of the robot are performed systematically both in simulations with the model and experiments with the robotic fish.

A. Simulations

By assigning the frequencies and amplitudes to the CPG controller, it outputs θ_i to be imported into the dynamic model. Specifically, by applying $f = 1$ Hz, $K_1 = K_2 = 0$, $K_3 = 20^\circ$ and $X_1 = X_2 = X_3 = 0$, forward swimming is performed in the simulation. Fig. 4(a) shows the simulated trajectory of the robot, where the robot moves in the positive-direction of the X-axis. Note that orientation of the robot is not strictly in line with the positive direction because that the forces acting on the robot is not perfectly symmetrical at the beginning time, as illustrated in Fig. 4(d) and 4(e) (The resultant forces in the X axis (F_x) and Y axis (F_y) are respectively equal to Q_x and Q_y). The oscillation of velocity (v_x) in X axis and the yaw angle (ψ) of robot demonstrate details of the swimming states of robotic fish, which is coincident with the motion description of swimming fish [16] and simulations in related paper [7], [8]. This partly demonstrates the relatively accuracy of the proposed AoA-based dynamic model. Fig. 4(f) shows that AoA is periodically variations when the robot is swimming.

Meanwhile, turning is induced by offering an offset for the tail. Parameter configurations are f = 1.2 Hz, $K_1 = K_2 = 0$, $K_3 = 20°$, $X_1 = X_2 = 0$ and $X_3 = 20°$. Figure 5(a) shows the simulated turning trajectory of the robot and the turning radius is around 0.6 m. Note that the trajectory is asymmetric about Y-axis, for the reason that a initial velocity in the X-axis is applied to avoid possible unstable states of the system at the start time. As illustrated in Fig. 5(b) and 5(c), it is apparent that asymmetric AoA of the tail results in asymmetric forces acting on the robot in y_b-axis, which further induces turning motion of the robot. The successful simulations for forward swimming and turning of the robot demonstrate the effectiveness of the AoA-based hydrodynamic modeling for the ostraciiform robotic fish.

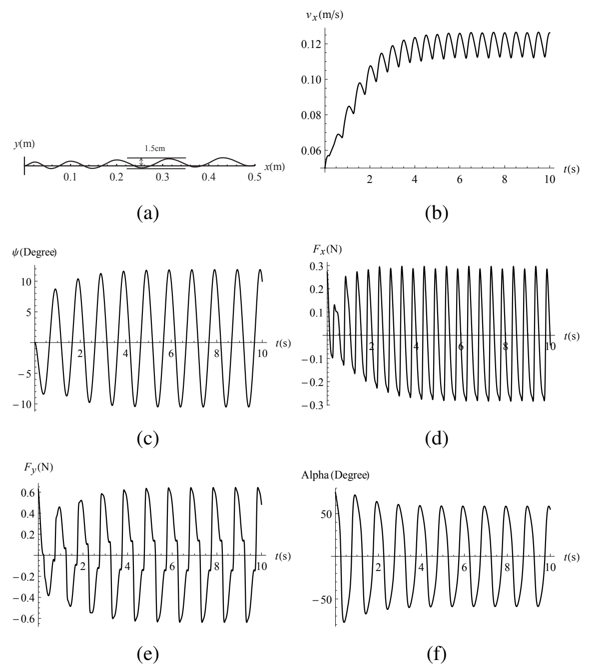

Fig. 4. Simulated forward swimming. (a) Forward swimming trajectory; (b) Oscillatory speed v_x of the robot; (c)Oscillatory yaw angle ψ; (d) Hydrodynamic forces acting on the X-axis; (e)Hydrodynamic forces acting on the Y-axis; (f) AoA of the tail.

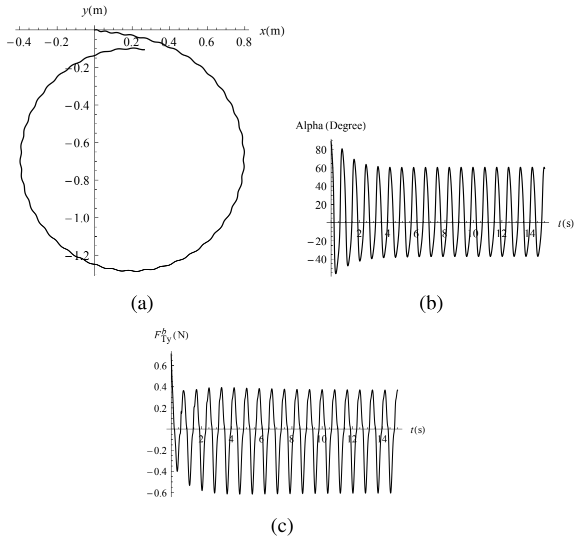

Fig. 5. Simulated turning of the robotic fish. (a)Trajectory of turning; (b)Hydrodynamic forces acting on the y_b-axis; (c) AoA of the tail.

B. Comparisons between Experiments and Simulations

To comprehensively show the effectiveness of the built AoA-based hydrodynamic model, experiments were systematically performed in a swimming tank (300 cm × 200 cm × 40 cm). An overhead HD camera is used to record image of robot and then velocity of robotic fish is obtained offline by a a vision tracking software. Meanwhile, yaw angle and accelerations of the robot is recorded online by an onboard IMU. Note that the experimental and simulated results have been run five times for a specific set of the imported CPG output signal θ_i.

Fig. 6 depicts the comparison results of forward swimming speed with $K_1 = K_2 = 0$ and $X_1 = X_2 = X_3 = 0$ but with different f and A_3. As presented in the figure, experimental results generally agree with the simulated velocity curve except that the robot swims with high frequencies ($f > 2.5$ Hz). The reason may be a simplified mechanical system, an inaccurate model and randomly selection of initial parameters in the simulation. Note also that the simulated speed is increasingly linear with the performed beating frequency, the reason could be that the forces acting on the robot are all quadratic with the robot's speed. This phenomenon could be avoided by taking more forces into consideration. However, considering the complexity of the AoA-based force analysis and dynamic model, and for the purpose of demonstrating the effectiveness of the AoA-based model, the proposed model is appropriate and effective to predict the mechanical behaviors of the robot with a variety of general used frequencies and amplitudes.

Furthermore, orientations and accelerations of the robot is recorded online to verify detailed characteristics (such as the variations of speed and lateral position) of the swimming states. The yaw angle illustrated in Fig. 7(a) shows the laterally sway of the robot just as the simulated curve in Fig. 4(c). Fig. 7(b) and (c) depict accelerations in x_b-axis and y_b-axis of the robot, which verify that the robot suffers variations of speed in one beating period. This agrees with

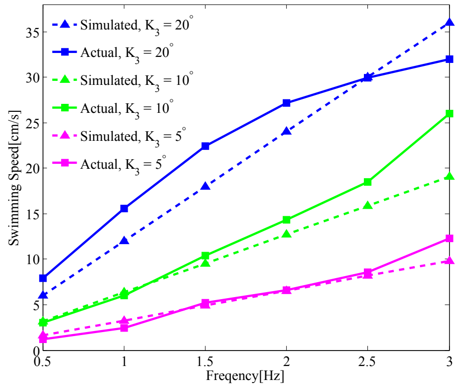

Fig. 6. Comparision of simulated and actual speeds of the robotic fish.

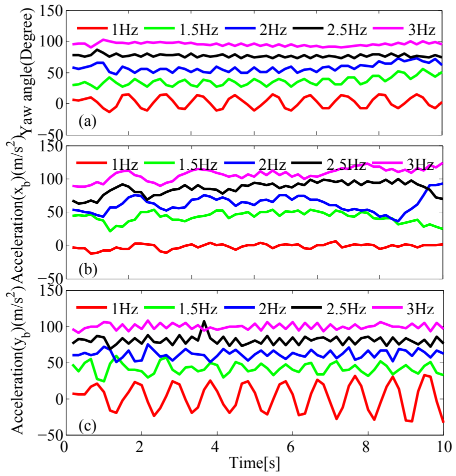

Fig. 7. The measured yaw angle and accelerations of the robot. To clearly display multi yaw angles and accelerations in one figure, the values for f = 1.5 Hz, 2 Hz, 2.5 Hz, 3 Hz have added the offsets of 40°, 60°, 80°, 100°, respectively. (a) Yaw angle; (b) Accelerations in x_b direction; (c) Accelerations in y_b direction.

the force simulations for the robot in Fig. 4(d) and 4(e). With careful observation, we can see that magnitude of the accelerations in y_b-axis are larger than that of values in x_b-axes, implying that the periodic lateral forces acting on the fish robot are more intensive than the forces acting on its travelling direction. This is also consistent with the results in Fig. 4(d) and 4(e). All of these detailed properties of fish states further verify the effectiveness of the whole AoA-based hydrodynamic analysis that primarily involving three types of forces.

V. Conclusion

This paper has established an AoA-based dynamic model for a CPG-controlled ostraciiform robotic fish with one paired pectoral fins and a caudal fin in a three-dimensional context. The CPG controller is used to produce signals of joint angle, which are further imported as the actuation of the multi-rigid-body robotic system. As an important factor in fish swimming, the explicit expression of the AoA is derived in this paper. Then using the quasi-steady wing theory, an AoA-based hydrodynamic model has been built for the multimodal swimming gaits of the robot. Comparative results between experiments and simulations have been performed to show the effectiveness of the proposed AoA-based dynamic model integrating with the CPG control law.

Further research will focus on realizing more swimming gaits simulations (such as backward swimming, pitching, rolling) based on the built 3D hydrodynamic model. In order to obtain a more accurate dynamic model for robotic fish, more fluid forces and more detailed modeling of the mechanical structure are worthy of investigation. Furthermore, more sensory feedback information will be imported to the CPG controller to improve the swimming performance and adaptations of the robotic fish.

Acknowledgment

References

[1] J. E. Colgate and K. M. Lynch, "Mechanics and control of swimming: A review," *IEEE Journal of Oceanic Engineering*, vol. 29, no. 3, pp. 660–673, 2004.

[2] D. T. Swain, I. D. Couzin, and N. E. Leonard, "Real-time feedback-controlled robotic fish for behavioral experiments with fish schools," *Proceedings of the IEEE*, vol. 100, no. 1, pp. 150–163, 2012.

[3] M. Lighthill, "Note on the swimming of slender fish," *J. Fluid Mech*, vol. 9, no. 2, pp. 305–317, 1960.

[4] M. J. Lighthill, "Large-amplitude elongated-body theory of fish locomotion," *Proceedings of the Royal Society B: Biological Sciences*, vol. 179, no. 1055, pp. 125–138, 1971.

[5] J. M. Anderson, K. Streitlien, D. S. Barrett, and M. S. Triantafyllou, "Oscillating foils of high propulsive efficiency," *Journal of Fluid Mechanics*, vol. 360, pp. 41–72, 1998.

[6] K. A. McIsaac and J. P. Ostrowski, "Motion planning for anguilliform locomotion," *Robotics and Automation, IEEE Transactions on*, vol. 19, no. 4, pp. 637–652, 2003.

[7] K. A. Morgansen, B. I. Triplett, and D. J. Klein, "Geometric methods for modeling and control of free-swimming fin-actuated underwater vehicles," *Robotics, IEEE Transactions on*, vol. 23, no. 6, pp. 1184–1199, 2007, robotics, IEEE Transactions on.

[8] J. Yu, M. Wang, Z. Su, M. Tan, and J. Zhang, "Dynamic modeling of a CPG-governed multijoint robotic fish," *Advanced Robotics*, vol. 27, no. 4, pp. 275–285, 2013.

[9] V. Kopman and M. Porfiri, "Design, modeling, and characterization of a miniature robotic fish for research and education in biomimetics and bioinspiration," *Mechatronics, IEEE/ASME Transactions on*, vol. 18, no. 2, pp. 471–483, 2013.

[10] G. Barbera, P. Lijuan, and D. Xinyan, "Attitude control for a pectoral fin actuated bio-inspired robotic fish," in *Robotics and Automation (ICRA), 2011 IEEE International Conference on*, ser. Robotics and Automation (ICRA), 2011 IEEE International Conference on, 2011, pp. 526–531.

[11] D. A. Read, F. S. Hover, and M. S. Triantafyllou, "Forces on oscillating foils for propulsion and maneuvering," *Journal of Fluids and Structures*, vol. 17, no. 1, pp. 163–183, 2003.

[12] Q. Zhu, M. J. Wolfgang, D. Yue, and M. S. Triantafyllou, "Three-dimensional flow structures and vorticity control in fish-like swimming," *Journal of Fluid Mechanics*, vol. 468, pp. 1–28, 2002.

[13] W. Wang, J. Guo, Z. Wang, and G. Xie, "Neural controller for swimming modes and gait transition on an ostraciiform fish robot," in *Advanced Intelligent Mechatronics (AIM), 2013 IEEE/ASME International Conference on*, ser. Advanced Intelligent Mechatronics (AIM), 2013 IEEE/ASME International Conference on, 2013, pp. 1564–1569.

[14] A. J. Ijspeert, A. Crespi, D. Ryczko, and J. M. Cabelguen, "From swimming to walking with a salamander robot driven by a spinal cord model," *Science*, vol. 315, no. 5817, pp. 1416–1420, 2007.

[15] A. J. Healey, S. M. Rock, S. Cody, D. Miles, and J. P. Brown, "Toward an improved understanding of thruster dynamics for underwater vehicles," *IEEE Journal of Oceanic Engineering*, vol. 20, no. 4, pp. 354–361, 1995.

[16] J. H. Arakeri, "Fluid mechanics of fish swimming," *Resonance*, vol. 14, no. 1, p. 32, 2009.